American College of Neuropsychopharmacology

www.nature.com/npp

ARTICLE

Check for updates

Sexually dimorphic prelimbic cortex mechanisms play a role in alcohol dependence: protection by endostatin

Yosef Avchalumov[1], Alison D. Kreisler[1], Nancy Xing[1], Amin A. Shayan[1], Tejash Bharadwaj[1], Jacob R. Watson[2], Britta Sibley[1], Sucharita S. Somkuwar[1], Wulfran Trenet[1,5], Sumaiya Olia[1], Juan C. Piña-Crespo[3], Marisa Roberto[3] and Chitra D. Mandyam[1,4]✉

Angiogenesis or proliferation of endothelial cells plays a role in brain microenvironment homeostasis. Previously we have shown enhanced expression of markers of angiogenesis in the medial prefrontal cortex during abstinence in an animal model of ethanol dependence induced by chronic intermittent ethanol vapor (CIE) and ethanol drinking (ED) procedure. Here we report that systemic injections of the angiogenesis inhibitor endostatin reduced relapse to drinking behavior in female CIE-ED rats without affecting relapse to drinking in male CIE-ED rats, and female and male nondependent ED rats. Endostatin did not alter relapse to sucrose drinking in both sexes. Endostatin reduced expression of platelet endothelial cell adhesion molecule-1 (PECAM-1) in all groups; however, rescued expression of tight junction protein claudin-5 in the prelimbic cortex (PLC) of female CIE-ED rats. In both sexes, CIE-ED enhanced microglial activation in the PLC and this was selectively prevented by endostatin in female CIE-ED rats. Endostatin prevented CIE-ED-induced enhanced NF-kB activity and expression and Fos expression in females and did not alter reduced Fos expression in males. Analysis of synaptic processes within the PLC revealed sexually dimorphic adaptations, with CIE-ED reducing synaptic transmission and altering synaptic plasticity in the PLC in females, and increasing synaptic transmission in males. Endostatin prevented the neuroadaptations in the PLC in females via enhancing phosphorylation of CaMKII, without affecting the neuroadaptations in males. Our multifaceted approach is the first to link PLC endothelial cell damage to the behavioral, neuroimmune, and synaptic changes associated with relapse to ethanol drinking in female subjects, and provides a new therapeutic strategy to reduce relapse in dependent subjects.

Neuropsychopharmacology (2021) 46:1937–1949; https://doi.org/10.1038/s41386-021-01075-6

INTRODUCTION

Endothelial cells are critical components of the blood–brain barrier. They form complex interactions with other resident cell types in the brain including neurons, microglia, astrocytes, and pericytes, to form the neurovascular unit [1]. Through angiogenesis and expression of junctional proteins, endothelial cells assist with the integrity of barrier properties and buffer against injury and disease [2]. Cell adhesion molecules are junctional proteins that maintain endothelial cell function [3]. Expression of platelet endothelial cell adhesion molecule-1 (PECAM-1) in endothelial cells is regulated by inflammatory stimuli, such that reducing PECAM-1 in animal models of ischemia and stroke suppressed leukocyte infiltration and exerted anti-inflammatory effects [4].

Moderate to severe alcohol use disorder (AUD) is a major risk factor for cerebrovascular diseases, in that AUD significantly increases both morbidity and mortality of stroke patients, particularly women [5, 6]. In vitro studies demonstrate that ethanol induces oxidative stress in endothelial cells, reduces expression of tight junction proteins, and promotes barrier dysfunction [7, 8]. In animal models, chronic ethanol exposure exacerbates inflammatory and vascular responses induced by focal ischemia [9]. We have previously demonstrated that escalated drinking patterns of ethanol consumption in an animal model of moderate to severe AUD followed by relapse to ethanol drinking during abstinence produced endothelial cell damage and barrier disruption, evident as increased expression of PECAM-1 and reduced expression of SMI-71 in the medial prefrontal cortex [10, 11]. While these studies reveal endothelial cell damage as a consequence of ethanol exposure, it is not clear if endothelial cell damage contributes to pathogenesis and progression of relapse drinking behaviors in individuals suffering from moderate to severe AUD.

To test this hypothesis, in the current study, we used a combination of histological, biochemical, and electrophysiological methods in an established adult rat model of moderate to severe AUD (chronic intermittent ethanol vapor with ethanol drinking, CIE-ED) in male and female rats to determine the protective effects of the FDA approved angiogenesis inhibitor endostatin [12, 13] on relapse to drinking behaviors. We examined the prelimbic region (PLC) of the medial prefrontal cortex, a key region that regulates relapse to ethanol drinking behaviors [14, 15]. CIE-ED consistently increased PECAM-1 expression and microglial activation in the PLC in both sexes, however, produced sexually dimorphic effects on the expression of tight junction protein claudin-5, oligodendrogenesis, neuronal activation, synaptic transmission and synaptic plasticity in the PLC. Endostatin reduced PECAM-1 expression in both sexes, however, prevented microglial activation, nuclear

[1]Veterans Affairs San Diego Healthcare System, San Diego, CA, USA. [2]Department of Psychology, California State University, Bakersfield, CA, USA. [3]Department of Molecular Medicine, Scripps Research, La Jolla, CA, USA. [4]Department of Anesthesiology, University of California San Diego, San Diego, CA, USA. [5]Deceased: Wulfran Trenet. ✉email: cmandyam@scripps.edu

Received: 2 April 2021 Revised: 12 June 2021 Accepted: 15 June 2021
Published online: 12 July 2021

factor kappa light chain enhancer of activated B cells (NF-kB) hyperexpression, hyperoligodendrogenesis, neuronal activation, and maladaptive synaptic effects in females which correlated with reduced relapse to drinking behaviors. Our multifaceted approach is the first to link PLC endothelial cell damage to the behavioral, neuroimmune, and synaptic changes associated with relapse to ethanol drinking in female subjects.

MATERIALS AND METHODS

Animals

One hundred and thirty-four adult female and ninety-nine adult male Long Evans rats (Charles River) completed the study. All rats were seven to eight weeks old at the beginning of the study, and females weighed ≈160–180 g and males weighed ≈220–240 g. The rats were maintained in reverse 12 h light-12h dark cycle rooms and housed two/cage unless otherwise specified. Food and water were available ad libitum. All experimental procedures were carried out in strict adherence to the National Institutes of Health Guide for the Care and Use of Laboratory Animals and were approved by the Institutional Animal Care and Use Committee at VA San Diego Healthcare System.

Ethanol Self-Administration (ethanol drinking, ED)

The behavioral experiments conducted herein are presented as a detailed schematic in Fig. 1a. One hundred and sixty-four experimentally-naïve rats were trained in the operant conditioning boxes (Med Associates Inc, VT), on a fixed-ratio 1 schedule for the delivery of 0.1 ml ethanol (10% v/v). Subsequently, the rats were divided into two groups; one group received chronic intermittent ethanol vapor exposure (CIE-ED; procedure details are provided in supplementary methods) while the other group (ED) was exposed to air in their normal housing condition (did not experience ethanol vapors) for a duration of six to seven weeks. The air pressure and ethanol flow rates were optimized to obtain blood alcohol levels (BALs) between 125 and 250 mg/dl or 27.2 and 54.4 mM [16]. For measuring BALs, tail bleeding was performed on the CIE-ED rats, once a week, between hours 13–14 of vapor exposure (Supplementary Fig. 1; Fig. S1; [16]). When plasma samples were outside the target range (125–250 mg/dl), vapor levels were adjusted accordingly. All rats received two 30-min FR1 sessions per week during these 6–7 weeks. Responding was analyzed to determine escalation of self-administration compared to prevapor stable responding. After 7 weeks of CIE, CIE-ED rats were withdrawn from ethanol vapors and both CIE-ED and ED rats were withdrawn from ethanol self-administration. Both CIE-ED and ED rats were divided into two groups (vehicle or endostatin) and maintained as described for the remainder of the study.

Endostatin Treatment

Endostatin (recombinant mouse endostatin) was purchased from a commercial source (BioLegend, Cat# 95453; 0.5 mg/ml). Endostatin was dissolved in sterile saline (vehicle). Endostatin or an equal volume of vehicle was injected at a dose of 0.3 mg/kg s.c. based on previous reports [12, 13, 17]. ED and CIE-ED ethanol rats and additional behavior naïve controls (ethanol naïve; $n = 26$ females and $n = 13$ males) were injected with saline or endostatin for five days. CIE-ED rats were given the first injection 2–3 h after the cessation of seven weeks of CIE, and ED and control rats were injected on the same day at the same time. Some control rats were euthanized to evaluate the expression of PECAM-1 either 72 h or four weeks after endostatin treatment (Fig. S2).

Relapse drinking during abstinence

After 23 days of abstinence from CIE and ethanol self-administration, CIE-ED and ED rats, both with and without endostatin, were given access to 30 min FR1 session to lever press for ethanol reinforcement (0.1 ml of 10% v/v ethanol) under cue-context conditions identical to that used for training and maintenance. Active and inactive lever responses were recorded. One hour following relapse, some animals were euthanized for electrophysiological analysis. Others experienced extinction and reinstatement sessions. One hour after reinstatement all animals were euthanized under anesthesia by rapid decapitation.

Sucrose self-administration

Sixteen female and sixteen male rats were trained to orally self-administer sucrose solution (10% sucrose on an FR1 schedule; context A) for the same number of sessions used in the ethanol self-administration paradigm. Details on this procedure are provided in supplementary methods.

Estrous cycle tracking

All female rats (controls, ethanol, and sucrose) were vaginally swabbed with a sterile cotton swab soaked in 0.9% saline after the last reinstatement session (CIE-ED and ED rats, or age-matched for controls) before euthanasia. Samples were applied to Superfrost® Plus slides and dried overnight and stained with Cresyl Echt Violet Solution (Abcam) to determine stage of estrous based on cell morphology [18] (Fig. S6).

Brain tissue collection for Western blotting and immunohistochemistry

The brains were removed and dissected along the midsagittal plane. The left hemisphere was snap-frozen for Western blotting analysis and the right hemisphere was postfixed in 4% paraformaldehyde for immunohistochemistry (IHC). Sections containing the PLC (+3.2 and +2.7 mm from bregma; area 32 according to [19]) were mounted and processed for PECAM-1, Olig2, Fos and Iba-1 IHC. Additional methodology for Western blotting and IHC are provided in the supplementary methods section and are based on our prior publication [11]. Details on quantitative analysis for PECAM-1, Ki-67, Olig2, Fos labeled cells are provided in the supplementary methods section. Absolute cell counting was performed in the PLC (counting of all immunoreactive cells in the contoured area); the data are presented as a total number of cells per unit area (cells/mm^2) per animal as the contoured area of PLC differed between subjects. Iba-1 labeled cells were traced in Neurolucida to create three-dimensional (3D) tracings that were analyzed with Neurolucida Explorer (MicroBrightField). Details on Iba-1 morphological analysis are provided in the supplementary methods section.

Slice preparation for electrophysiology

Brains were removed and placed in ice-cold artificial cerebrospinal fluid (ACSF) containing (in mM): 126 NaCl, 26 $NaHCO_3$, 2.5 KCl, 1.25 NaH_2PO_4, 2 $CaCl_2$, 1.25 $MgCl_2$ and 10 glucose bubbled with 95% oxygen and 5% CO_2 [20]. Brains were trimmed on the dorsal side at an angle of ≈140° from the horizontal plane and glued to a vibratome base (Leica VT1000S). Thick slices (440 µm) containing the PLC were obtained and used for recordings. Three to four slices were transferred to a submerged chamber and incubated with oxygenated ACSF at 25 °C for at least 1–1.5 h before initiating recordings. Recordings were made in the PLC (Fig. 4a, b), in a submersion-type recording chamber superfused with oxygenated ACSF at a rate of 2–3 ml/min at 32 °C and positioned on the stage of an upright motorized microscope (Olympus BX51 WI, Scientifica) equipped with a back Illuminated sCMOS camera (Prime 95B, Photometrics) and a broad-spectrum LED illuminator (pE-300, CoolLED).

Field potential recordings

To study basal synaptic transmission and paired-pulse ratio (PPR) under vehicle (DMSO or 0.1 N NaOH) conditions, local field potentials were recorded in acute brain slices in the presence of $GABA_A$ receptor antagonist bicuculline methiodide [21] (BMI, 1 µM; Sigma). Field excitatory postsynaptic potentials (fEPSPs) were evoked by extracellular stimulation (0.03 Hz, 0.2 ms) in the PLC using a silver-coated tungsten wire stimulating electrode (50 µm, A-M System; Fig. 4b) placed in the deep layer of PLC (layer II/III) in line with the recording electrode. fEPSPs were recorded using ACSF-filled patch pipettes with tip resistances of 2–4 MΩ. Pipettes were pulled from borosilicate glass capillaries (PG150T-10, Harvard Apparatus) using a micropipette puller (PC-10, Narishige). At least three slices per rat were used for recordings.

Basal synaptic transmission was analyzed by generating stimulus/response curves or input/output (I/O) curves prior to each synaptic plasticity experiment. I/O curves were generated by plotting stimulus intensity (100–900 µA) versus fEPSP slope (Fig. S9; [22]). The slope of fEPSPs was measured after the stimulus artifact and the fiber volley from the initial 2–5 ms of the rising phase to about half-peak time of the synaptic response. For the remainder of the experiment, the test stimulus intensity was set to elicit a fEPSP that is ≈40–50% of the maximum response recorded during the I/O measurements. Paired-pulse ratios (P2/P1) were evaluated by dividing the slope of second fEPSP by the slope of first fEPSP obtained at 50 ms inter-stimulus interval (Fig. 4c). fEPSPs at this constant test stimulus intensity were monitored for a period of 25 min to ensure stable responses before induction of LTP.

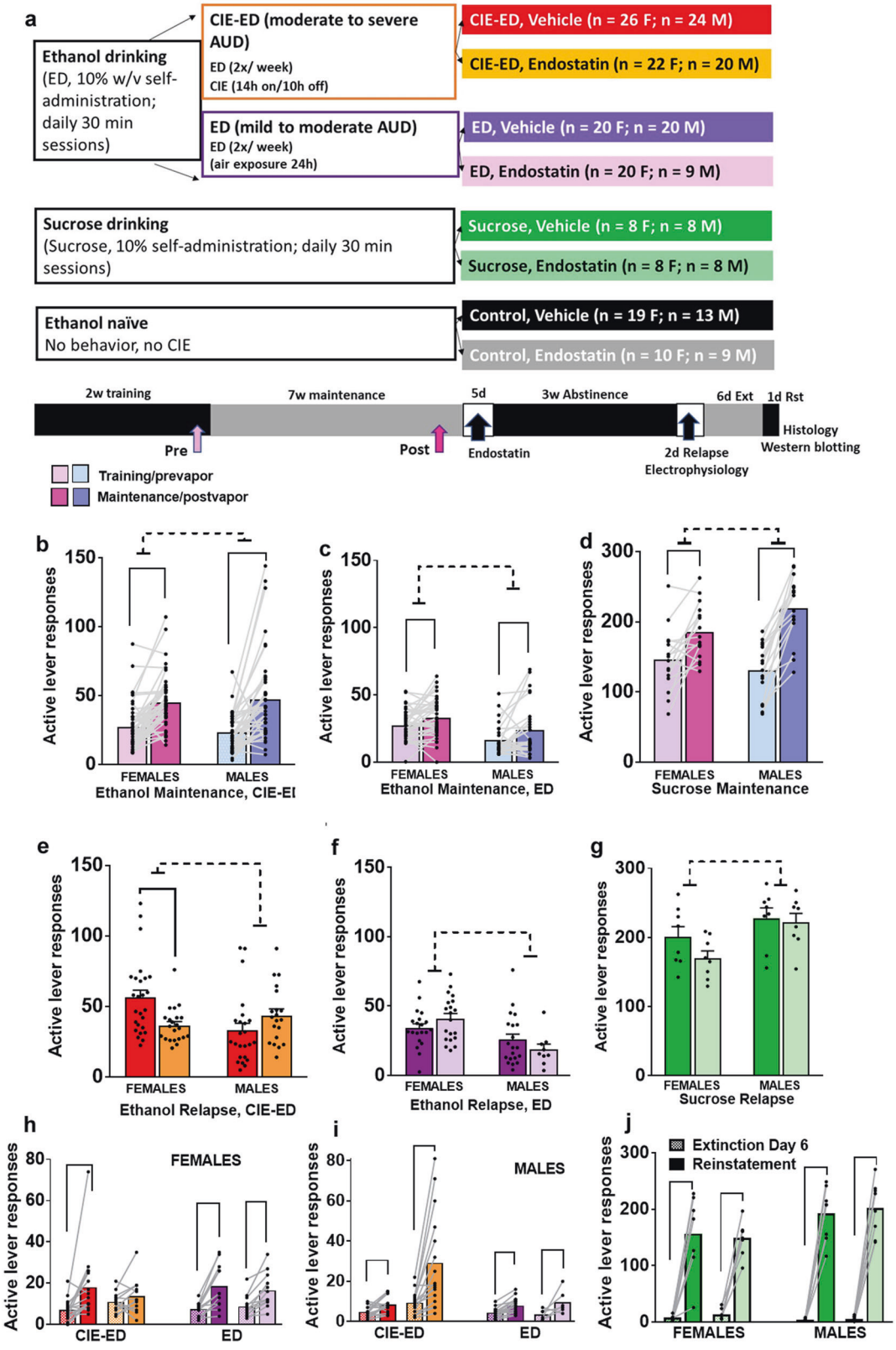

For induction of synaptic plasticity or long-term potentiation LTP in the PLC, the following high-frequency stimulation HFS stimulation paradigm was used: four trains of HFS (100 pulses at 50 Hz per train) delivered 10 s apart [21]. Experiments assessing the role of GluNs in HFS-LTP were conducted in the presence of (2 R)-amino-5-phosphonovaleric acid [23] (APV; 30 μM, Sigma) in addition to BMI. APV was bath applied 5 min prior to induction of LTP and remained until the end of the experiment. Experiments assessing the role of GluAs in HFS-LTP were conducted in the presence of 6,7-Dinitroquinoxaline-2,3(1H,4H)-dione [21] (DNQX; 20 μM, Sigma) in addition to BMI. DNQX was bath applied 5 min prior to induction of LTP and remained until the end of the experiment. For comparisons of treatment effects on fEPSP slope between slices, values for each recording

Fig. 1 Behavioral data of ethanol and sucrose rats during training, maintenance, relapse, and reinstatement sessions. a Experimental timeline and experimental groups used in the current study. **b–d** Active lever responses of female and male rats for ethanol or sucrose consumption during training (prevapor) or maintenance (postvapor) sessions. Active lever responding was compared between last three days of training and last week of maintenance in female and male ED and female and male sucrose rats that did not experience CIE. Arrows in the timeline indicate the time of sessions used for generating graphs (**b–d**). **b** In CIE-ED rats, repeated measures two-way ANOVA detected a main effect of CIE (F (1, 87) = 66.6; $p < 0.001$) without a CIE x sex interaction or main effect of sex. Pairwise comparisons also indicated higher active lever responses during last week of maintenance in female and male CIE-ED rats compared with last days of training. **c** In ED rats, repeated measures two-way ANOVA demonstrated a main effect of time (F (1, 66) = 14.5; $p = 0.003$) and main effect of sex (F (1, 66) = 11.5; $p = 0.0012$) without a time x sex interaction. Pairwise comparisons indicated higher active lever responses in female ED rats compared with male ED rats during the pre and post sessions. Pairwise comparisons also indicated higher active lever responses during the last week of maintenance in female and male ED rats compared with last days of training. Inactive lever responses did not differ between sexes and over time. **d** In sucrose rats, repeated measures two-way ANOVA demonstrated a time x sex interaction (F (1, 30) = 9.4; $p = 0.004$), main effect of time (F (1, 30) = 64.7; $p < 0.001$) without a main effect of sex. Post hoc analysis indicated higher active lever responses during the last week of maintenance in female and male sucrose rats compared with last days of training. Post hoc analysis also indicated higher active lever responses in male sucrose rats compared with female rats during the post sessions. Inactive lever responses did not differ between ethanol and sucrose groups (Fig. S3). Endostatin reduces relapse to drinking behavior in female CIE-ED rats. **e** In CIE-ED rats, two-way ANOVA demonstrated a sex x endostatin interaction (F (1, 88) = 10.77; $p = 0.001$), a trend towards main effect of sex (F (1, 88) = 3.1, $p = 0.08$) without main effect of endostatin. Post hoc analysis showed reduced active lever responses in CIE-ED-endostatin female rats compared to vehicle controls, and reduced active lever responses in CIE-ED-saline male rats compared to CIE-ED-saline female rats ($ps < 0.05$). Endostatin does not alter relapse to drinking behavior in female and male ED and sucrose rats. **f** In ED rats, two-way ANOVA demonstrated a strong trend towards sex x endostatin interaction (F (1, 65) = 3.0; $p = 0.08$), a main effect of sex (F (1, 65) = 14.5, $p = 0.003$) without main effect of endostatin. Pairwise comparisons indicated higher active lever responses in ED-endostatin female rats compared with ED-endostatin male rats ($p < 0.05$). **g** In sucrose rats, two-way ANOVA demonstrated a main effect of sex (F (1, 28) = 8.6; $p = 0.006$) without a sex x endostatin interaction and main effect of endostatin. Pairwise comparisons indicated higher active lever responses in sucrose–endostatin male rats compared with sucrose–endostatin female rats ($p < 0.05$). Inactive lever responses did not differ between groups. Endostatin reduces reinstatement of ethanol-seeking behavior in female CIE-ED rats. Following six days of extinction, the rats were subject to contextual cued reinstatement. Ethanol and sucrose seeking behavior were separately analyzed in female and male groups with behavior days (extinction vs. reinstatement) as within-subject factor and endostatin as between-subject factor. **h** In female CIE-ED rats repeated measures two-way ANOVA detected a main effect of reinstatement (F (1, 28) = 8.9; $p = 0.005$), with a trend towards reinstatement x endostatin interaction (F (1, 28) = 3.1; $p = 0.08$), and without main effect of endostatin. Pairwise comparisons indicated higher responding during reinstatement in vehicle treated CIE-ED females compared with extinction session ($p < 0.05$). This effect was abolished in endostatin treated CIE-ED female rats. In female ED rats repeated measures two-way ANOVA detected a main effect of reinstatement (F (1, 22) = 41.5; $p < 0.001$), without a reinstatement x endostatin interaction or main effect of endostatin. Pairwise comparisons indicated higher responding during reinstatement in vehicle and endostatin treated ED females compared with extinction session ($ps < 0.05$). **i** In male CIE-ED rats repeated measures two-way ANOVA detected a reinstatement x endostatin interaction (F (1, 31) = 10.1; $p = 0.003$), a main effect of reinstatement (F (1, 31) = 21.3; $p < 0.001$), and main effect of endostatin (F (1, 31) = 13.0; $p = 0.001$). Post hoc analysis indicated higher responding during reinstatement in endostatin treated CIE-ED males compared with extinction session ($p < 0.05$). This effect was not evident in vehicle treated CIE-ED male rats. In male ED rats repeated measures two-way ANOVA detected a main effect of reinstatement (F (1, 20) = 19.4; $p = 0.003$), without a reinstatement x endostatin interaction or main effect of endostatin. Pairwise comparisons indicated higher responding during reinstatement in vehicle and endostatin treated ED males compared with extinction session ($ps < 0.05$). **j** In female sucrose rats repeated measures two-way ANOVA detected a main effect of reinstatement (F (1, 13) = 109.6; $p < 0.001$), without a reinstatement x endostatin interaction or main effect of endostatin. Pairwise comparisons indicated higher responding during reinstatement in vehicle and endostatin treated sucrose females compared with extinction session ($ps < 0.05$). In male sucrose rats repeated measures two-way ANOVA detected a main effect of reinstatement (F (1, 14) = 292.1; $p < 0.001$), without a reinstatement x endostatin interaction or main effect of endostatin. Pairwise comparisons indicated higher responding during reinstatement in vehicle and endostatin treated ED males compared with extinction session ($ps < 0.05$). Data are expressed as mean ± SEM. Females: $n = 26$ CIE-ED-vehicle, $n = 22$ CIE-ED-endostatin, $n = 20$ ED-vehicle, $n = 20$ ED-endostatin, $n = 8$ sucrose-vehicle, $n = 8$ sucrose–endostatin. Males: $n = 24$ CIE-ED-vehicle, $n = 20$ CIE-ED-endostatin, $n = 20$ ED-vehicle, $n = 9$ ED-endostatin, $n = 8$ sucrose-vehicle, $n = 8$ sucrose–endostatin.

were normalized to the average slope for the 10 min of baseline before HFS was initiated. Data was acquired, filtered (highpass, 0.1 Hz; lowpass 3 kHz), and amplified using a computer-controlled patch-clamp amplifier (MultiClamp 700B, Molecular Devices) and digitized using an analog to digital converter (Digidata 1550A1, Molecular Devices). Analysis of fEPSP slope was performed using pClamp10.4 software (Molecular Devices).

Statistical Analysis

Ethanol self-administration CIE-ED female and male rats, ethanol self-administration in female and male ED rats, and sucrose self-administration in female and male rats were evaluated using repeated measures two-way ANOVA with the session (or time) as a within-subject factor and sex as a between-subject factor. Differences in ethanol self-administration between CIE-ED and ED rats were evaluated using repeated measures two-way ANOVA with the session (or time) as a within-subject factor and CIE as a between-subject factor in each sex. Differences in BALs between female and male CIE-ED rats were evaluated using repeated measures two-way ANOVA with week (or time) as a within-subject factor and sex as a between-subject factor. Effect of endostatin on relapse to drinking and reinstatement in each condition (CIE-ED, ED, or sucrose) was evaluated with endostatin and sex as a between-subject factor. Significant interactions were followed by Fisher's LSD post hoc tests. When interactions were not evident, pairwise comparisons were performed to determine group or sex differences. Histological and biochemical measures were compared between control, ED, and CIE-ED rats with vehicle or endostatin treatment within each sex using two-way ANOVAs, followed by post hoc tests. Active lever responses and Fos were correlated with histological and biochemical markers using Pearson's product-moment correlation coefficient. Similarly, electrophysiological data were compared between control, ED, and CIE-ED rats with vehicle or endostatin treatment within each sex using two-way ANOVAs, followed by post hoc tests. Behavioral scores during endostatin injections over the five days were compared using a nonparametric Mann-Whitney test. Statistical significance was accepted at $p < 0.05$.

RESULTS

CIE enhances blood alcohol levels (BAL) and ethanol drinking during maintenance in female and male rats

A schematic of the timeline of experimental design and experimental groups is indicated in Fig. 1a. BALs in CIE-ED rats steadily increased starting week 4 compared with week 1, and BAL was maintained between 150–300 g/dL in CIE-ED rats between weeks four and seven (Fig. S1). Active lever responding was compared between last three days of training and last week of maintenance under the influence of CIE in female and male CIE-ED rats. Active lever responding for ethanol significantly increased after CIE in female and male CIE-ED

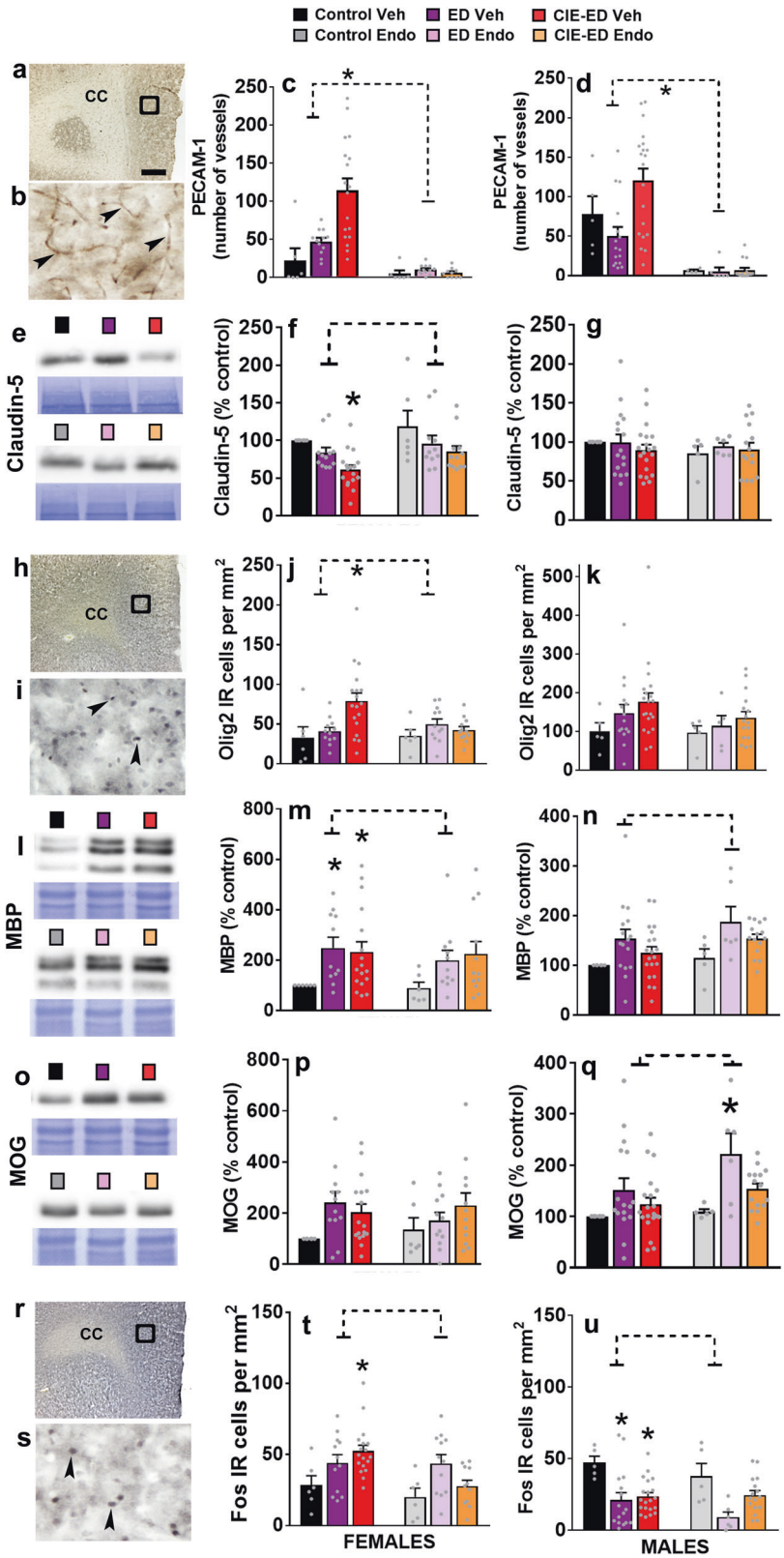

rats during the maintenance phase ($p < 0.05$; Fig. 1b). Inactive lever responding did not differ between the time points in both sexes (Fig. S3). Female and male, ED and sucrose animals show enhanced operant responding during maintenance ($p < 0.05$; Fig. 1c, d). CIE-ED rats have enhanced ethanol drinking behavior during maintenance compared with ED rats in both sexes ($p < 0.05$; Fig. 1a, b).

Endostatin reduces relapse to drinking behavior in female CIE-ED Rats

We first determined whether endostatin alters behavioral responses during injection sessions in female and male CIE-ED rats, as published reports indicate that forced withdrawal from CIE-ED induces significant physical withdrawal behavior [16].

Fig. 2 CIE-ED sex specifically alters expression of endothelial junction proteins, oligodendrocytes, myelin and neuronal activity in the PLC and endostatin prevents these effects. Immunohistrochemistry was performed to determine the effects of endostatin on PECAM-1, Olig-2, and Fos expression. Western blotting was performed to determine the effects of endostatin on claudin-5, MBP, and MOG expression. Two-way ANOVA was performed with groups (control, CIE-ED, and ED) and endostatin treatment (saline, endostatin) as between-subject factors. **a**–**d** PECAM-1: **a**, **b** 25x Low magnification (**a**) and 200x high magnification image (**b**) of PECAM-1 cells in the PLC from one CIE-ED female rat. Area in the PLC used for cell quantification is indicated as a black square in (**a**). cc corpus callosum. Scale bar in (**a**) is 200 μm, applies to (**a**, **h**, **r**). **c** In females, two-way ANOVA showed a significant group x endostatin interaction (F (2, 58) = 7.8; $p = 0.001$), main effect of endostatin (F (1, 58) = 26.8; $p < 0.002$) and group (F (2, 58) = 7.2; $p = 0.01$). Post hoc analysis showed enhanced expression of PECAM-1 in CIE-ED-saline rats compared with all other groups ($ps < 0.05$). **d** In males, two-way ANOVA showed a significant group x endostatin interaction (F (2, 60) = 3.3; $p = 0.04$), main effect of endostatin (F (1, 60) = 31.2; $p < 0.001$) and group (F (2, 60) = 3.6; $p = 0.03$). Post hoc analysis showed enhanced expression of PECAM-1 in CIE-ED-saline rats compared with ED-saline, ED-endostatin, control-endostatin, and CIE-ED-endostatin ($ps < 0.05$) and a strong trend compared with control saline ($p = 0.06$). **e**–**g** Claudin-5: (**e**) Immunoreactive bands of claudin-5 from female rats detected at 25 kDa. Staining for coomassie is indicated as it was used as a loading control. **f** In females, there was a significant main effect of group (F (2, 58) = 6.8; $p = 0.002$) and endostatin (F (1, 58) = 5.2; $p = 0.02$), without a group x endostatin interaction. Pairwise comparisons showed reduced expression of claudin-5 in CIE-ED-saline rats compared with all other groups ($ps < 0.05$). **g** In males, claudin-5 was unaltered. **h**–**k** Olig2: **h**, **i** 25x Low magnification (**h**) and 200x high magnification (**i**) image of Olig2 cells in the PLC from one female CIE-ED rat. Area in the PLC used for cell quantification is indicated as a black square in (**h**). cc corpus callosum. **j** In females, a significant group x endostatin interaction (F (2, 60) = 4.4; $p = 0.01$), main effect of group (F (2, 60) = 4.0; $p = 0.02$), without a main effect of endostatin on the number of Olig2 cells was detected. Post hoc analysis showed an enhanced number of Olig2 cells in CIE-ED-saline rats compared with all other groups ($ps < 0.05$). **k** In males, Olig2 cells were unaltered. **l**–**n** MBP: (**e**) Immunoreactive bands of MBP detected at 18–23 kDa from female rats. Staining for coomassie is indicated as it was used as a loading control. **m** In females, a significant main effect of group (F (2, 57) = 4.1; $p = 0.02$), without group x endostatin interaction or the main effect of endostatin on the expression of MBP was detected. Pairwise comparisons showed enhanced expression of MBP in CIE-ED-saline and ED-saline rats compared with vehicle and endostatin controls ($ps < 0.05$). **n** In males, a significant main effect of group, without group x endostatin interaction or a main effect of endostatin on the expression of MBP (F (2, 63) = 4.7; $p = 0.01$) was detected. Pairwise comparisons showed enhanced expression of MBP in ED-endostatin rats compared with controls ($ps < 0.05$). **o**–**q** MOG: (**o**) Immunoreactive bands of MOG detected at 25 kDa from female rats. Staining for coomassie is indicated as it was used as a loading control. **p** In females, expression of MOG was unaltered. **q** In males, a significant main effect of group, without group x endostatin interaction or a main effect of endostatin on the expression of MOG (F (2, 62) = 5.7; $p = 0.004$) was detected. Pairwise comparisons showed enhanced expression of MOG in ED-endostatin rats compared with all other groups ($ps < 0.05$). **r**–**u** Fos: **r**, **s** 25x Low magnification (**r**) and 200x high magnification (**s**) image of Fos cells in the PLC from one female CIE-ED rat. Area in the PLC used for cell quantification in indicated as a black square in (**r**). cc corpus callosum. **t** In females, a significant group x endostatin interaction (F (2, 59) = 3.0; $p = 0.05$), main effect of group (F (2, 59) = 4.9; $p = 0.01$), and endostatin (F (1, 59) = 5.2; $p = 0.02$) on the number of Fos cells was detected. Post hoc analysis showed enhanced number of Fos cells in CIE-ED-saline rats compared with control groups and CIE-ED-endostatin rats ($ps < 0.05$). **u** In males, a significant main effect of group (F (2, 62) = 10.6; $p = 0.001$), without group x endostatin interaction or a main effect of endostatin on the number of Fos was detected. Pairwise comparisons showed reduced number of Fos cells in CIE-ED and ED rats compared with controls ($ps < 0.05$). Data are expressed as mean ± SEM. Females: $n = 6$ control-vehicle, $n = 6$ control-endostatin, $n = 16$–18 CIE-ED-vehicle, $n = 8$–10 CIE-ED-endostatin, $n = 10$–12 ED-vehicle, $n = 10$–12 ED-endostatin. Males: $n = 5$ control-vehicle, $n = 5$ control-endostatin, $n = 18$–20 CIE-ED-vehicle, $n = 13$–15 CIE-ED-endostatin, $n = 14$–16 ED-vehicle, $n = 6$ ED-endostatin.

Endostatin reduces behavioral responses during injection sessions (Fig. S5). Following four weeks of forced abstinence, drinking behavior was assessed in CIE-ED, ED, and sucrose rats that experienced vehicle or endostatin. Endostatin reduced relapse to drinking behavior in CIE-ED females and did not alter relapse to drinking behavior in ED females, CIE-ED and ED males, and sucrose rats (Fig. 1e–g). CIE-ED-vehicle female rats have enhanced ethanol drinking behavior during relapse compared with ED-vehicle female rats and this effect is absent with endostatin ($p < 0.05$; Fig. 1e, f). Endostatin reduces contextual cued reinstatement of ethanol seeking in female CIE-ED rats and enhances reinstatement of ethanol seeking in male CIE-ED rats ($p < 0.05$; Fig. 1h, i). Endostatin did not alter reinstatement of ethanol seeking in female and male ED rats and did not alter reinstatement of sucrose seeking in female and male rats (Fig. 1h–j).

Taken together, our behavioral data support the sexually dimorphic effects of endostatin on relapse drinking and reinstatement of ethanol-seeking behavior in CIE-ED rats. In addition, since there were group differences between CIE-ED and ED conditions that were evident during maintenance, relapse, and reinstatement, we evaluated the effect of vehicle (saline) and endostatin under CIE-ED and ED conditions in each sex separately, on all histological, biochemical and electrophysiological analysis in the PLC (Figs. 2–5). We also evaluated the effect of vehicle and endostatin in sucrose rats on all histological and biochemical measures (Fig. S10).

Endostatin reduces PECAM-1 expression but differentially alters claudin-5 expression, oligodendrogenesis, neuronal activation, and neuroimmune responses in the PLC in female and male ED and CIE-ED rats

In vehicle CIE-ED females and males, there was a significant increase in PECAM-1 compared to controls and ED rats. Endostatin generally reduced PECAM-1 expression in all groups in both the sexes ($p < 0.05$; Fig. 2c, d). In vehicle CIE-ED females claudin-5 was significantly reduced, and endostatin prevented this effect ($p < 0.05$; Fig. 2f, g). In males, claudin-5 was unaltered. In vehicle CIE-ED females, there was a significant increase in Olig2 expression compared to controls and ED rats. Endostatin reduced Olig2 expression in females ($p < 0.05$; Fig. 2j, k). In males, Olig2 was unaltered. In females and males, there was a main effect of ethanol experience on MBP expression. In vehicle ED and CIE-ED females, MBP expression was higher than controls. This effect was not significant with endostatin (Fig. 2m, n). MOG expression was unaltered in females. In vehicle ED and CIE-ED males, MOG expression was higher than controls, and this was unaltered with endostatin (Fig. 2p, q). In vehicle ED and CIE-ED rats, Fos was bidirectionally altered with increases in females and decreases in males. Endostatin rescued the effects in females and did not alter the effects in males ($p < 0.05$; Fig. 2t, u).

We evaluated the state of Iba-1-labeled microglia (ramification, total process length, area of cell soma) in female and male CIE-ED and ED rats under vehicle and endostatin conditions, as these morphological characteristics define the activity state of these cells [24]. We found reduced process ramification and total process length in vehicle female and male CIE-ED rats. These morphological changes reveal the activated state of Iba-1-labeled microglia. In addition, in vehicle CIE-ED females, enhanced area of cell soma of Iba-1-labeled cells was evident. In females, endostatin normalized the morphological changes in CIE-ED rats to control levels ($p < 0.05$; Fig. 3d–f). We then determined whether the activity state of microglial cells in female CIE-ED rats occurred coincidentally with activity and expression of the transcription factor NF-kB, as it regulates inflammation and innate immunity and plays a role in neuroinflammatory responses in AUD [25, 26]. Western blot

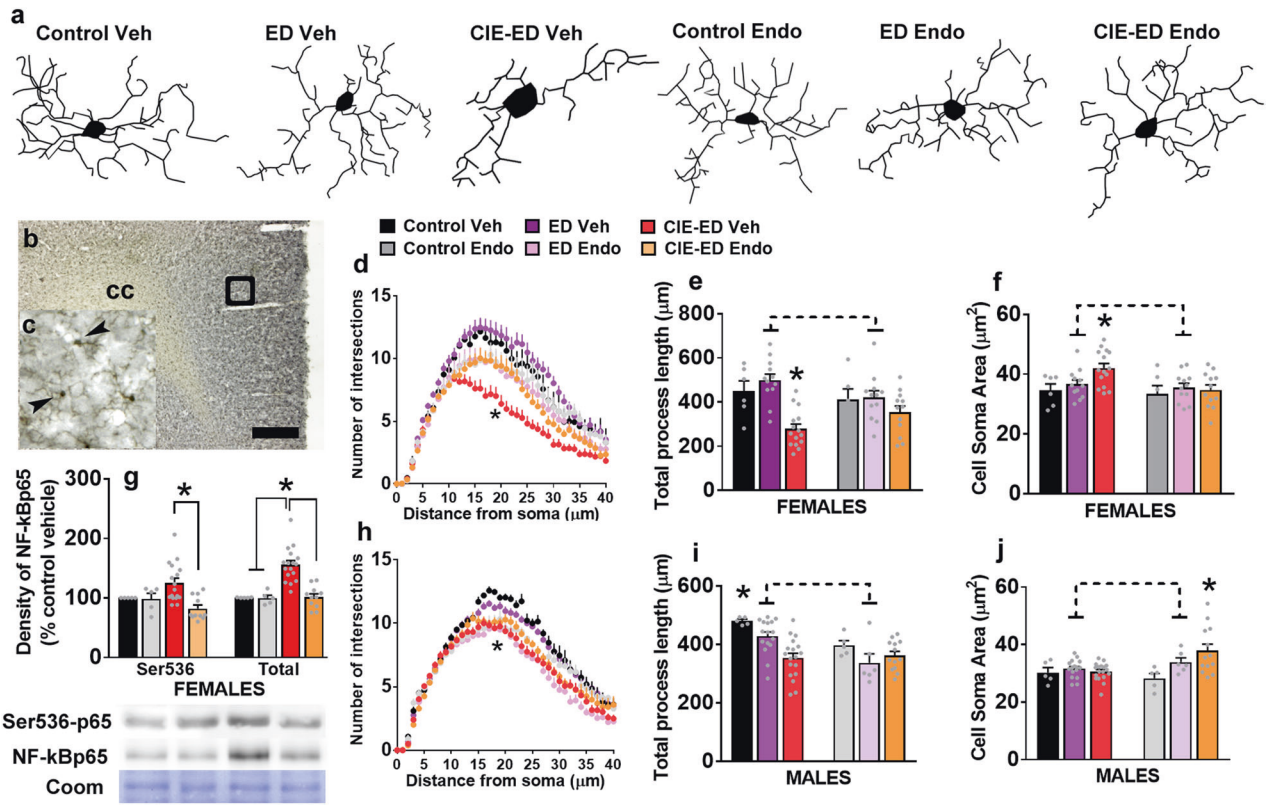

Fig. 3 CIE-ED increases neuroimmune responses in female and male rats; endostatin prevents this effect selectively in females. a 3D tracings of Iba-1 labeled microglial cells in the PLC from six experimental groups from female rats. **b**–**c** 25x Low magnification (**b**) and 200x high magnification image (**c**) of Iba-1 cells in the PLC from one control female rat. Area in the PLC used for cell quantification is indicated as a black square in (**b**). cc corpus callosum. Scale bar in (**b**) is 200 μm. **d**–**f** In females, repeated measures two-way ANOVA detected a group x distance from soma interaction (F (200, 2280) = 3.1; $p < 0.001$), main effect of distance from soma (F (40, 2280) = 250.4; $p < 0.001$), and main effect of group (F (5, 57) = 6.2; $p = 0.001$). Post hoc analysis revealed lower ramification in CIE-ED-vehicle group compared to all other groups and lower ramification in ED-endostatin group compared to ED-vehicle group. **e** Two-way ANOVA revealed a main effect of group (F (2, 59) = 9.0; $p = 0.004$) without an endostatin x group interaction or main effect of endostatin in total dendrite length. Pairwise comparisons revealed lower process length in CIE-ED-vehicle rats compared with all other rats. **f** Two-way ANOVA revealed a main effect of endostatin (F (1, 57) = 4.7; $p = 0.03$) and a strong trend towards main effect of group (F (2, 57) = 2.7; $p = 0.07$) without an endostatin x group interaction in cell soma area. Pairwise comparisons revealed higher cell soma area in CIE-ED-vehicle rats compared with all other rats. **g** Quantitative data of phosphorylated NF-kBp65 Ser536 and total NF-kBp65 indicated as percent change from control-vehicle group in females. One-way ANOVA indicated a significant effect of CIE in phosphorylated (F (3, 33) = 6.4; $p = 0.001$) and total NF-kB (F (3, 33) = 18.7; $p = 0.001$) expression in CIE-ED rats. Post hoc analysis revealed higher expression of phosphorylated NF-kB in CIE-ED-vehicle rats compared with CIE-ED-endostatin rats and higher expression of NF-kB in CIE-ED-vehicle rats compared with all other groups ($p < 0.05$). Example immunoblots of NF-kB from each experimental group. Coomassie stain was used as a loading control. **h**–**j** In males, repeated measures two-way ANOVA detected a group x distance from soma interaction (F (200, 2400) = 1.7; $p < 0.001$), main effect of distance from soma (F (40, 2400) = 342.8; $p < 0.001$), and main effect of group (F (5, 60) = 4.8; $p = 0.008$). Post hoc analysis revealed lower ramification in CIE-ED-vehicle and CIE-ED-endostatin group compared controls and ED-saline groups. In addition, ED-endostatin rats showed reduced ramification compared with ED-saline rats. **h** Two-way ANOVA revealed a endostatin x group interaction (F (2, 57) = 4.8; $p = 0.01$), a main effect of group (F (2, 57) = 7.0; $p = 0.001$) and main effect of endostatin (F (1, 57) = 10.3; $p = 0.002$) in total process length. Post hoc analysis revealed higher process length in control-vehicle rats compared with all other rats. **i** Two-way ANOVA revealed endostatin x group interaction (F (2, 57) = 4.0; $p = 0.02$), main effect of group (F (2, 57) = 4.1; $p = 0.02$) and a strong trend towards a main effect of endostatin (F (1, 57) = 3.3; $p = 0.07$) in cell soma area. Post hoc analyses revealed higher cell soma area in CIE-ED-endostatin rats compared with all other rats. Data are expressed as mean ± SEM. Females: $n = 6$ control-vehicle, $n = 6$ control-endostatin, $n = 16$–18 CIE-ED-vehicle, $n = 8$–10 CIE-ED-endostatin, $n = 10$–12 ED-vehicle, $n = 10$–12 ED-endostatin. Males: $n = 5$ control-vehicle, $n = 5$ control-endostatin, $n = 18$–20 CIE-ED-vehicle, $n = 13$–15 CIE-ED-endostatin, $n = 14$–16 ED-vehicle, $n = 6$ ED-endostatin.

analyses of NF-kBp65 were conducted on PLC tissue lysates. CIE-ED enhanced activity and expression of NF-kB in the PLC and endostatin prevented this effect (Fig. 3g). In males, endostatin did not alter the morphological changes in CIE-ED rats, and therefore, maintained the activated state of these cells (Fig. 3h–j).

Electrophysiological analysis reveals distinct effects of endostatin on synaptic transmission and synaptic plasticity in the PLC in CIE-ED and ED female and male rats

We recorded evoked field excitatory postsynaptic potentials (fEPSPs) in PLC layer II/III (Fig. 4a, b) to assess potential effects of relapse to ethanol seeking and endostatin on basal synaptic transmission using a range of stimulus intensities (Fig. S8). We evaluated the input/output (I/O) curves in control, ED, and CIE-ED with vehicle or endostatin in females and males. In vehicle CIE-ED females, I/O curve was reduced and this was normalized with endostatin ($p < 0.05$; Fig. S8). I/O curve was unaffected in males.

We also evaluated the effects of endostatin on paired-pulse ratios (PPR) of fEPSPs (at 50 ms inter-stimulus interval) in female and male, control, CIE-ED, and ED rats. Changes in PPR are inversely related to transmitter release such that enhanced

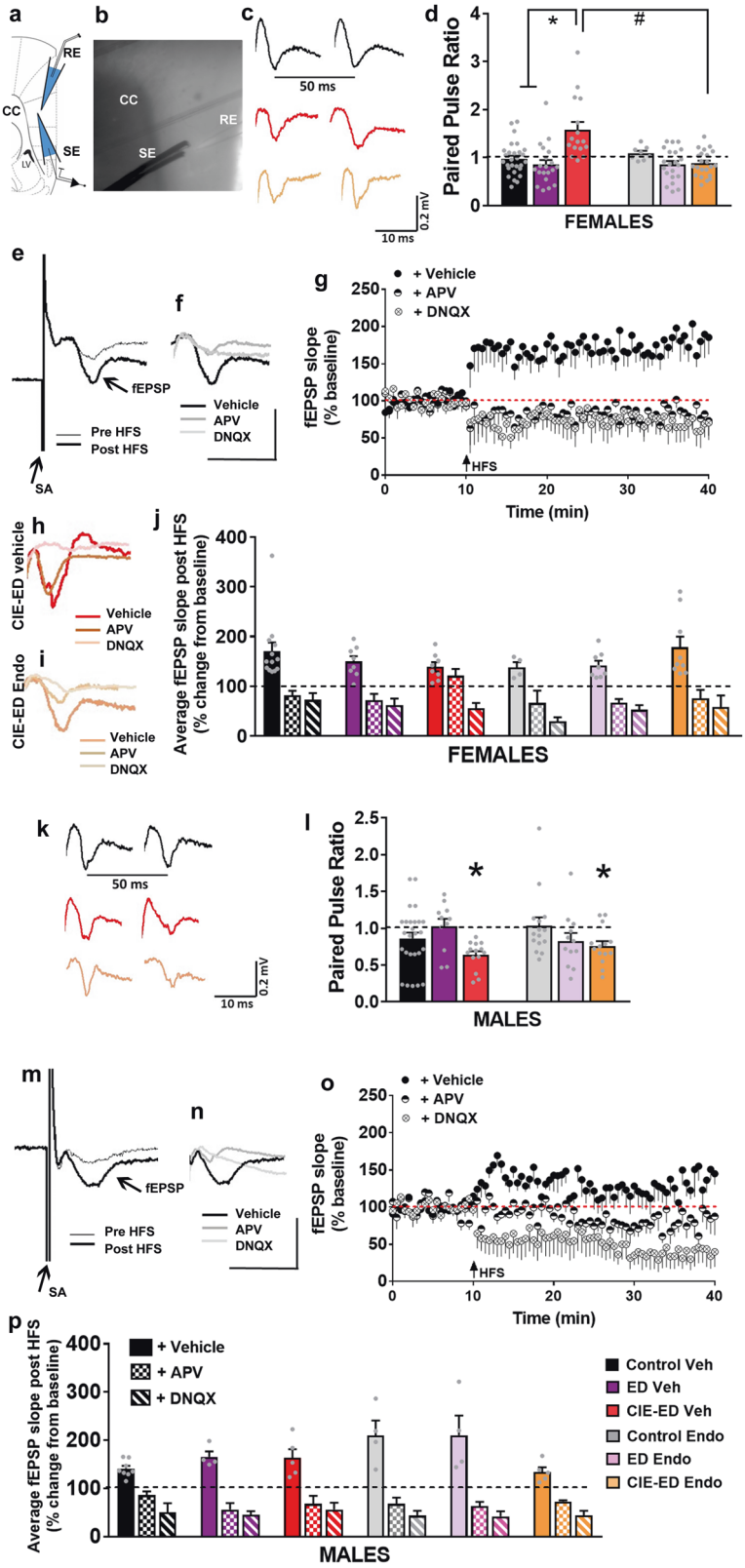

probability of transmitter release is associated with a reduction of PPR, whereas the decreased probability of transmitter release is associated with an increase in PPR [27, 28]. In vehicle CIE-ED females, we observed increased PPR or paired-pulse facilitation compared to all other groups, suggesting decreased glutamate release. Notably, this was completely abolished with endostatin ($p < 0.05$; Fig. 4c, d). In contrast, vehicle CIE-ED males displayed reduced PPR or paired-pulse depression compared to controls and ED groups, suggesting increased glutamate release. This effect, however, remained with endostatin (Fig. 4l).

Fig. 4 CIE-ED produces distinct effects on synaptic activity and long-term potentiation induced by high-frequency stimulation in the PLC in females and males; endostatin selectively prevents these effects in females. a Section of the rat brain at Bregma 2.7 mm and typical placement of the stimulating and recording electrodes in layers V and II/III, respectively, in the PLC. **b** Representative slice used for recordings with the stimulating electrode (SE) and recording electrode (RE) placements. cc corpus callosum. **c** Representative traces of paired-pulse stimulations in the PLC from female control-vehicle, CIE-ED-vehicle, and CIE-ED-endostatin rats. fEPSPs were generated at 50 ms intervals and stimulus artifacts were removed for clarity. **d** Paired-pulse ratio shown as mean ± SEM from all-female experimental groups. In females, two-way ANOVA indicated a significant group x endostatin interaction (F (2, 115) = 12.5; $p < 0.001$), main effect of endostatin (F (1, 115) = 6.8; $p = 0.01$) and group (F (2, 115) = 9.7; $p = 0.001$). Post hoc analysis indicated higher PPR in CIE-ED-vehicle treated rats compared with all other groups ($p < 0.05$). **e** Representative traces of normalized fEPSPs before (pre) and after (post) HFS from control-vehicle female rat. Traces are indicated with stimulus artifact (SA). **f** Representative traces of normalized fEPSPs post HFS with vehicle, APV, and DNQX in control-vehicle rat. Scale bar is 0.5 mV and 10 ms. **g** fEPSP slope shown as mean ± SEM from all-female control-vehicle group. Repeated measures two-way ANOVA detected a significant time x treatment interaction (F (162, 1701) = 3.2; $p < 0.0001$) and main effect of drug treatment (F (2, 21) = 10.3; $p = 0.008$) without detecting a main effect of time post HFS. Post hoc analysis revealed higher fEPSP slopes in vehicle condition compared with APV and DNQX ($ps < 0.05$). **h, i** Representative traces of normalized fEPSPs post HFS with vehicle, APV, and DNQX from CIE-ED-vehicle (**h**) and CIE-ED-endostatin (**i**) rats. **j** Average fEPSP slope post HFS (40 min) shown as mean ± SEM from all-female experimental groups. In females, two-way ANOVA did not indicate a group x endostatin interaction, main effect of group or endostatin in vehicle condition. Applications of DNQX completely blocked LTP in control, ED and CIE-ED groups under vehicle and endostatin treatments in female ($ps < 0.05$). In female rats, application of APV completely blocked LTP in control and ED groups in vehicle and endostatin conditions ($p < 0.05$). In CIE-ED-saline rats, application of APV did not block LTP; however, this effect was rescued in CIE-ED-endostatin rats ($p < 0.05$). **k** Representative traces of paired-pulse stimulations in the PLC from male control-vehicle, CIE-ED-vehicle, and CIE-ED-endostatin rats. fEPSPs were generated at 50 ms intervals and stimulus artifacts were removed for clarity. **l** Paired-pulse ratio shown as mean ± SEM from all-male experimental groups. In males, two-way ANOVA indicated a main effect of group (F (2, 86) = 4.3; $p = 0.01$) without significant group x endostatin interaction or main effect of endostatin. Pairwise comparisons indicated lower PPR in CIE-ED-vehicle and CIE-ED-endostatin treated rats compared with control-endostatin rats ($p < 0.05$). **m** Representative traces of normalized fEPSPs before (pre) and after (post) HFS from control-vehicle male rat. Traces are indicated with stimulus artifact (SA). **n** Representative traces of normalized fEPSPs post HFS with vehicle, APV and DNQX. Scale bar is 0.5 mV and 10 ms. **o** fEPSP slope shown as mean ± SEM from all-male control-vehicle group. Repeated measures two-way ANOVA detected a significant time x treatment interaction (F (162, 1134) = 2.3; $p < 0.0001$), main effect of time (F (81, 1134) = 1.3; $p = 0.03$), and main effect of drug treatment (F (2, 14) = 11.6; $p = 0.001$) post HFS. Post hoc analysis revealed higher fEPSP slopes in vehicle condition compared with APV and DNQX ($p < 0.05$). **p** Average fEPSP slope post HFS (40 min) shown as mean ± SEM from all-male experimental groups. In males, two-way ANOVA revealed a significant group x endostatin interaction (F (2, 25) = 4.1; $p = 0.02$), main effect of endostatin (F (1, 25) = 4.0; $p = 0.05$) without a main effect of group. Post hoc analysis revealed higher LTP in control-endostatin and ED-endostatin groups compared with CIE-ED-endostatin group ($p < 0.05$). Following applications of APV and DNQX, we observed a complete blockade of LTP in control, ED, and CIE-ED groups under vehicle and endostatin treatments ($ps < 0.05$). Data are expressed as mean ± SEM. Number of rats, Females: $n = 5$–13 control-vehicle, $n = 2$–4 control-endostatin, $n = 4$–8 CIE-ED-vehicle, $n = 4$–9 CIE-ED-endostatin, $n = 6$–8 ED-vehicle, $n = 6$–8 ED-endostatin. Number of slices for PPR, Females: $n = 28$ control-vehicle, $n = 8$ control-endostatin, $n = 16$ CIE-ED-vehicle, $n = 22$ CIE-ED-endostatin, $n = 20$ ED-vehicle, $n = 21$ ED-endostatin. Slices for LTP, Females: $n = 5$–13 control-vehicle, $n = 8$ control-endostatin, $n = 4$–8 CIE-ED-vehicle, $n = 4$–9 CIE-ED-endostatin, $n = 6$–8 ED-vehicle, $n = 6$–8 ED-endostatin. Number of rats, Males: $n = 5$–8 control-vehicle, $n = 4$ control-endostatin, $n = 5$ CIE-ED-vehicle, $n = 5$ CIE-ED-endostatin, $n = 3$–4 ED-vehicle, $n = 4$ ED-endostatin. Slices for PPR, Males: $n = 26$ control-vehicle, $n = 15$ control-endostatin, $n = 14$ CIE-ED-vehicle, $n = 14$ CIE-ED-endostatin, $n = 11$ ED-vehicle, $n = 12$ ED-endostatin. Slices for LTP, Males: $n = 4$–8 control-vehicle, $n = 4$–5 control-endostatin, $n = 5$ CIE-ED-vehicle, $n = 5$ CIE-ED-endostatin, $n = 4$ ED-vehicle, $n = 4$ ED-endostatin.

Lastly, we also measured the degree of LTP as the average of the fEPSP slope after a 40 min period of post-HFS recording in the PLC in control, ED, and CIE-ED groups with vehicle or endostatin in female and male rats (Fig. 4j, p). We first demonstrate that the expression of LTP in the PLC in female and male rats under control conditions is dependent on activation of GluN and GluA receptors (Fig. 4g, o). The degree of LTP was not altered by ethanol under ED and CIE-ED conditions in female and male rats (Fig. 4j,p). To further investigate the underlying LTP mechanisms in each group, we tested whether GluN or GluA signaling was involved in HFS-induced plasticity in the PLC, in control, ED, and CIE-ED groups with vehicle or endostatin by inhibiting GluN or GluA signaling prior to the HFS paradigm. Following applications of DNQX, we observed a complete blockade of LTP in control, ED, and CIE-ED groups under vehicle and endostatin in female and male rats (Fig. 4j, p). In females, following applications of APV we observed complete blockade of LTP in control and ED groups in vehicle and endostatin conditions (Fig. 4j). Although in vehicle CIE-ED females, application of APV did not block LTP, endostatin rescued this effect (Fig. 4j). In males, following applications of APV we observed complete blockade of LTP in control, ED, and CIE-ED groups in vehicle and endostatin conditions (Fig. 4p). We then determined a mechanism for endostatin's effect on PPR and rescue of GluN mediated LTP in female CIE-ED rats (Fig. 5). Western blot analyses of pCaMKII and tCaMKII were conducted on PLC tissue lysates. Endostatin enhanced expression of pCaMKII in the PLC at the autophosphorylation site in female CIE-ED rats without altering tCaMKII expression (Fig. 5a,b).

DISCUSSION

A growing number of in vitro and in vivo studies demonstrate that ethanol alters the expression of endothelial cell junction proteins and disrupts blood–brain barrier function [8, 10, 11, 29]. Thus, here we investigated the sexually dimorphic role of PECAM-1, a junction protein of endothelial cells in relapse to ethanol drinking using the well-established CIE-ED rat model of ethanol dependence that produces behavioral, neurobiological, and transcriptional changes that overlap with those found in moderate to severe AUD. We also included an established ED model of mild AUD and sucrose drinking to determine PECAM-1 depletion on nondependent ethanol drinking and sucrose drinking. Moreover, histological, biochemical, and electrophysiological analyses in the PLC provided important mechanistic insight into how PECAM-1 depletion impacts alcohol dependence-induced neuroadaptations and behavioral changes in each sex.

Findings from clinical studies demonstrate significant gender differences in the neurotoxic effects and cognitive impairing effects of alcohol in individuals suffering from mild to severe AUD [30–32], with women being more vulnerable. Therefore, our evaluation of ED and CIE-ED effects on cellular and neurobiological alterations in the PLC in both sexes is highly significant. CIE-ED increased PECAM-1 expression in the PLC in both sexes, and this was reduced by endostatin. Although ED and sucrose drinking did not increase PECAM-1 expression in the PLC, endostatin reduced PECAM-1 expression in both groups. Notably, PECAM-1 depletion prevented dependence-induced enhanced relapse to ethanol drinking and seeking in CIE-ED rats, without altering relapse to ethanol drinking in nondependent ED rats and relapse

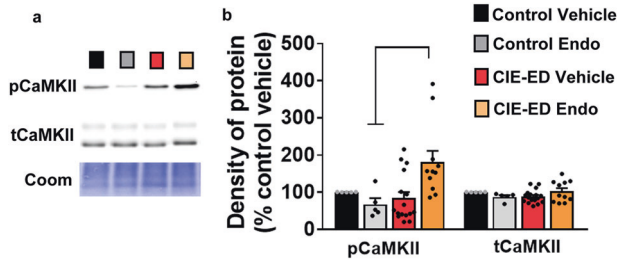

Fig. 5 Endostatin significantly increases pCaMKII levels in the PLC in female CIE-ED rats. a Example immunoblots of pCaMKII and tCaMKII from each experimental group. Coomassie stain was used as a loading control. **b** Quantitative data of pCaMKII and tCaMKII indicated as percent change from control-vehicle group. One-way ANOVA indicated a significant effect of endostatin in pCaMKII expression in CIE-ED rats (F (3, 33) = 4.9; $p = 0.006$). Post hoc analysis revealed higher expression of pCaMKII in CIE-ED-endostatin rats compared with all other groups ($p < 0.05$). One-way ANOVA did not detect a significant difference in tCaMKII. Data are expressed as mean ± SEM. $n = 5$ control-vehicle, $n = 5$ control-endostatin, $n = 16$ CIE-ED-vehicle, $n = 11$ CIE-ED-endostatin.

to sucrose drinking in females. This novel finding supports the hypothesis that enhanced expression of PECAM-1 during abstinence is necessary to drive dependence-induced relapse to drinking in female subjects. While our findings do not show a mechanistic role of PECAM-1 in relapse to drinking in male subjects, enhanced PECAM-1 expression in males may be a consequence of escalated ethanol consumption.

Increased PECAM-1 expression occurred in concert with reduced expression of claudin-5 in females. Claudin-5 is highly expressed in brain endothelial cells [33], and functions to enhance the structural integrity of the endothelial cells to prevent barrier leakage. Depletion of claudin-5 is associated with exacerbated inflammatory and lymphatic responses [34] and, in turn, inflammatory cytokines deplete claudin-5 expression [35, 36]. Furthermore, endostatin prevented claudin-5 depletion, suggesting that PECAM-1 may be producing divergent immune responses in female and male PLC to alter relapse to ethanol drinking [37, 38].

In vivo studies have demonstrated that endothelial damage or angiogenesis in the context of ischemia or stroke increases oligodendrogenesis [39–41]. More notable is the white matter vulnerability to endothelial cell damage [39, 42], visualized as enhanced expression of myelin-associated proteins. We previously demonstrated enhanced proliferation of oligodendroglial progenitors in the prefrontal cortex, which occurred coincidentally with increased expression of myelin-associated proteins and PECAM-1 in male CIE-ED rats [11]. We also reported that abstinence-induced increases in myelin-associated proteins in the medial prefrontal cortex in male CIE rats were aberrant and resulted in flayed dysfunctional myelin [43]. Here, we extend these findings in female rats, to show increases in oligodendrogenesis and myelin-associated proteins in the PLC and demonstrate a mechanistic role of PECAM-1 in regulating these effects. Furthermore, it appears that, in males, oligodendrogenesis and myelin dysfunction were not linked to endothelial cell damage in the PLC, further supporting the sexually dimorphic mechanisms underlying dependence-induced relapse to drinking.

The increases in PECAM-1 occurred in concert with the activation of microglial cells in the PLC in both sexes, albeit to a higher degree in female rats. Our findings support previous observations in both rodent and human studies of AUD-induced enhanced microglial activity in several regions of the brain [24, 44–48], and provide correlative evidence for a role of endothelial damage in ethanol-induced neuroimmune responses in both sexes. In males, microglial responsiveness to CIE in the PLC is higher than other brain regions implicated in ethanol reinforcement and relapse [24]. Furthermore, in males, microglial responsiveness in the prefrontal cortex translates to microglial-mediated neural circuit adaptation following CIE and enhanced drinking behavior during withdrawal [45]. The current findings add to these mechanistic results to demonstrate the sex-specific role of endothelial damage in microglial responsiveness in the PLC, and that microglial activation in the PLC played a role in enhanced relapse to drinking during abstinence in females.

The increases in PECAM-1 and NF-kBp65 in females occurred coincidentally, and endostatin reduced the expression and activation of NF-kB. With respect to NF-kB, several interesting evidence demonstrates that PECAM-1 could enhance NF-kB expression, and conversely, NF-kB could increase the transcription of PECAM-1. For example, it is important to note that PECAM-1 regulation of NF-kB occurs under conditions of oxidative stress-induced inflammation [49, 50], and does not occur in in vitro conditions that involve mere overexpression of PECAM-1 [51]. With respect to NF-kB regulation of PECAM-1, molecular studies have identified two consensus sites for NF-kB within the promotor region of PECAM-1 gene [52]. A few studies have demonstrated functional relevance for this interaction, where NF-kB regulates transcriptional activity of PECAM-1 [53], and vascular inflammation mediated by PECAM-1 is dependent on NF-kB activity [54]. Given the evidence that NF-kB is implicated in the neuroinflammatory responses in AUDs [55, 56] and that PECAM-1 could be involved in the neuroinflammatory responses in AUD [10, 11], the current findings show a sex-specific relationship between PECAM-1 and NF-kB in the PLC, and that NF-kB activation and expression in the PLC is associated with enhanced relapse to drinking during abstinence in females. Endostatin reduced the expression and activity of NF-kB in the PLC and supported the previously demonstrated effect of endostatin on NF-kB in pure endothelial cells [57]. Future studies are warranted to define the sex-specific inflammatory and immune-related genes and responses in endothelial cells in the PLC under CIE-ED and ED conditions. In this context, a potential limitation in the interpretation of our findings is that changes in the expression of astrocytes were not examined. These studies are important as recent gene network analysis in mice in the prefrontal cortex has revealed gene expression changes in astrocytes and microglia in response to CIE that could regulate the alcohol-dependent phenotype [45, 58]. Even more interesting is that astrocytes play a role in maintaining the neurovascular niche and are key players in the pathogenesis of vascular diseases [59, 60]. Therefore, examining the role of reactive astrocytes and their role in sex-specific inflammatory and immune-related genes and responses in the PLC under CIE-ED and ED conditions is an important future pursuit.

We also examined the neuroadaptations in the PLC in both sexes that occurred as a consequence of relapse to drinking. Analysis of neuronal activity with Fos revealed bidirectional changes in the PLC in females compared with males, with CIE-ED females having enhanced Fos expression and CIE-ED males having reduced Fos expression. Endostatin reduced Fos expression in CIE-ED females, indicating a role for PECAM-1 in modulating neuronal activity in the PLC. Endostatin did not alter Fos expression in males, emphasizing the sexually dimorphic role of PECAM-1 in regulating neuronal activity in the PLC. Given the role of glutamatergic signaling in AUD [61–63], we then assessed potential adaptations at PLC glutamatergic synapses. Our electrophysiological data in CIE-ED-vehicle females revealed a reduced I/O curve and increased paired-pulse ratio of fEPSPs indicating reduced synaptic transmission and reduced glutamate release in the PLC [27, 28]. In contrast, results in CIE-ED-vehicle males revealed enhanced glutamate release in the PLC. The increased Fos expression and reduced glutamate release in CIE-ED females may reflect homeostatic adaptation of glutamatergic synapses in

the PLC in response to ethanol cues and seeking behaviors [64, 65]. Endostatin enhanced the expression of phosphorylated CaMKII in the PLC and prevented the adaptations in CIE-ED females. These findings suggest that endothelial damage promotes ethanol-induced homeostatic modulation via presynaptic effects. Endostatin rescued these effects, perhaps by regulating CaMKII activity at the presynaptic sites [66] or functioning as a trans-synaptic signal controlling neurotransmitter release [67], and this correlated with reduced relapse to drinking behaviors. Although delineating a molecular mechanism for endostatin's effects on CaMKII is beyond the scope of the current study, endostatin's modulatory effects on voltage-gated calcium channels could be facilitating the activity of CaMKII [68, 69]. Alternatively, the reduced Fos expression and increased glutamate release in CIE-ED males may reflect metaplastic changes in mechanisms that regulate presynaptic function that occurred during abstinence and seeking behaviors [70, 71]. Regardless of the exact mechanism driving the bidirectional changes in neuronal activity and synaptic transmission in the PLC, our study highlights the importance of examining sexually dimorphic synaptic responses in the context of ethanol-seeking behaviors.

Ethanol dependence impairs cognitive processes of learning and memory and memory processes at the synaptic level, including LTP, a well-characterized form of activity-dependent plasticity [27, 72–75]. One aspect of homeostatic adaptation to ethanol dependence may be dysregulation of HFS-LTP in the PLC. In females and males, we demonstrate that ethanol experience – under ED and CIE-ED conditions did not alter the degree of LTP compared to controls [76]. We further investigated the mechanism underlying LTP in the PLC. In female and male controls, we demonstrate that LTP in the PLC was prevented in the presence of GluN and GluA receptor antagonists, indicating that the PLC LTP is dependent on GluN and GluA receptor activation in both sexes. We additionally investigated whether the mechanism underlying LTP was altered in ED and CIE-ED rats in females and males. This is important as glutamatergic dysregulation via GluNs plays a role in alcohol dependence-induced neuroimmune, behavioral and functional characteristics [45, 61, 77, 78]. Our findings show that while GluN- and GluA-dependent LTP was preserved in female ED and male ED and CIE-ED rats, GluN-dependent LTP was dysregulated in female CIE-ED rats. This adaptation could play a role in mediating homeostatic plasticity in the PLC in female-dependent rats. Endostatin prevented this effect and rescued GluN-dependent LTP in female CIE-ED rats. These findings suggest that enhanced PECAM-1 and associated endothelial damage promoted or assisted with altered glutamatergic signaling in the PLC. It is also possible that endothelial damage assisted with neuroadaptive changes that were evident under low demand synaptic function including pre-HFS baseline responses and high demand synaptic function such as HFS-induced LTP. Conversely, ethanol-induced glutamate toxicity in the PLC could have contributed to endothelial damage in a GluN-dependent manner [10, 72, 79–82].

In summary, our multidisciplinary study is the first to show extensive effects of endostatin, from reduced relapse to drinking behavior in ethanol-dependent females, to reversal of oligodendroglial, microglial, neuroimmune, and synaptic adaptations in the PLC. A potential limitation in the interpretation of this work is that the molecular mechanisms for endostatin's protective effect are unclear and could be multidimensional. For example, endostatin's antiangiogenic effects may be due to its interactions with vascular endothelial growth factor receptors, integrin receptors, glypican receptors, androgen receptors, cell surface-associated proteins, and voltage-gated calcium channels [69, 83, 84]. Nevertheless, these findings suggest a complex, sex-specific role for PECAM-1 in the development of alcohol dependence.

REFERENCES

1. Muoio V, Persson PB, Sendeski MM. The neurovascular unit - concept review. Acta physiologica (Oxf, Engl). 2014;210:790–8.
2. Hawkins BT, Davis TP. The blood-brain barrier/neurovascular unit in health and disease. Pharm Rev. 2005;57:173–85.
3. Newman PJ. The biology of PECAM-1. J Clin Invest. 1997;99:3–8.
4. Woodfin A, Voisin MB, Nourshargh S. PECAM-1: a multi-functional molecule in inflammation and vascular biology. Arterioscler Thromb Vasc Biol. 2007; 27:2514–23.
5. Patra J, Taylor B, Irving H, Roerecke M, Baliunas D, Mohapatra S, et al. Alcohol consumption and the risk of morbidity and mortality for different stroke types-a systematic review and meta-analysis. BMC public health. 2010;10:258.
6. Schuckit MA. Alcohol-use disorders. Lancet 2009;373:492–501.
7. Haorah J, Heilman D, Knipe B, Chrastil J, Leibhart J, Ghorpade A, et al. Ethanol-induced activation of myosin light chain kinase leads to dysfunction of tight junctions and blood-brain barrier compromise. Alcohol Clin Exp Res. 2005;29:999–1009.
8. Haorah J, Knipe B, Leibhart J, Ghorpade A, Persidsky Y. Alcohol-induced oxidative stress in brain endothelial cells causes blood-brain barrier dysfunction. J Leukoc Biol. 2005;78:1223–32.
9. Fontes-Júnior EA, Maia CS, Fernandes LM, Gomes-Leal W, Costa-Malaquias A, Lima RR, et al. Chronic Alcohol Intoxication and Cortical Ischemia: Study of Their Comorbidity and the Protective Effects of Minocycline. Oxid Med Cell Longev. 2016;2016:1341453.
10. Somkuwar SS, Fannon MJ, Bao Nguyen T, Mandyam CD. Hyper-oligodendrogenesis at the vascular niche and reduced blood-brain barrier integrity in the prefrontal cortex during protracted abstinence. Neuroscience 2017;362:265–71.
11. Somkuwar SS, Fannon-Pavlich MJ, Ghofranian A, Quigley JA, Dutta RR, Galinato MH, et al. Wheel running reduces ethanol seeking by increasing neuronal activation and reducing oligodendroglial/neuroinflammatory factors in the medial prefrontal cortex. Brain Behav Immun. 2016;58:357–68.
12. Gertz K, Priller J, Kronenberg G, Fink KB, Winter B, Schrock H, et al. Physical activity improves long-term stroke outcome via endothelial nitric oxide synthase-dependent augmentation of neovascularization and cerebral blood flow. Circ Res. 2006;99:1132–40.
13. Shichiri M, Hirata Y. Antiangiogenesis signals by endostatin. Faseb j. 2001;15: 1044–53.
14. Palombo P, Leao RM, Bianchi PC, de Oliveira PEC, Planeta CDS, Cruz FC. Inactivation of the prelimbic cortex impairs the context-induced reinstatement of ethanol seeking. Front Pharmacol. 2017;8:725.
15. Dayas CV, Liu X, Simms JA, Weiss F. Distinct patterns of neural activation associated with ethanol seeking: effects of naltrexone. Biol Psychiatry. 2007;61: 979–89.
16. Gilpin NW, Richardson HN, Cole M, Koob GF. Vapor inhalation of alcohol in rats. Curr Protoc Neurosci. 2008;9:1–19. Chapter
17. Sorensen DR, Read TA. Delivery of endostatin in experimental cancer therapy. Int J Exp Pathol. 2002;83:265–74.
18. Cora MC, Kooistra L, Travlos G. Vaginal Cytology of the Laboratory Rat and Mouse: Review and Criteria for the Staging of the Estrous Cycle Using Stained Vaginal Smears. Toxicol Pathol. 2015;43:776–93.
19. Vogt BA, Paxinos G. Cytoarchitecture of mouse and rat cingulate cortex with human homologies. Brain Struct Funct. 2014;219:185–92.
20. Avchalumov Y, Sander SE, Richter F, Porath K, Hamann M, Bode C, et al. Role of striatal NMDA receptor subunits in a model of paroxysmal dystonia. Exp Neurol. 2014;261:677–84.
21. Kang S, Cox CL, Gulley JM. High frequency stimulation-induced plasticity in the prelimbic cortex of rats emerges during adolescent development and is associated with an increase in dopamine receptor function. Neuropharmacology 2018;141:158–66.
22. Petersen RP, Moradpour F, Eadie BD, Shin JD, Kannangara TS, Delaney KR, et al. Electrophysiological identification of medial and lateral perforant path inputs to the dentate gyrus. Neuroscience 2013;252:154–68.
23. Calabresi P, Gubellini P, Centonze D, Picconi B, Bernardi G, Chergui K, et al. Dopamine and cAMP-regulated phosphoprotein 32 kDa controls both striatal long-term depression and long-term potentiation, opposing forms of synaptic plasticity. J Neurosci. 2000;20:8443–51.
24. Siemsen BM, Landin JD, McFaddin JA, Hooker KN, Chandler LJ, Scofield MD. Chronic intermittent ethanol and lipopolysaccharide exposure differentially alter Iba1-derived microglia morphology in the prelimbic cortex and nucleus accumbens core of male Long-Evans rats. J Neurosci Res. 2020. https://pubmed.ncbi.nlm.nih.gov/32621337/.
25. Zou J, Crews F. Induction of innate immune gene expression cascades in brain slice cultures by ethanol: key role of NF-κB and proinflammatory cytokines. Alcohol Clin Exp Res. 2010;34:777–89.
26. Neumann M, Naumann M. Beyond IkappaBs: alternative regulation of NF-kappaB activity. Faseb j. 2007;21:2642–54.

27. Roberto M, Nelson TE, Ur CL, Gruol DL. Long-term potentiation in the rat hippocampus is reversibly depressed by chronic intermittent ethanol exposure. J Neurophysiol. 2002;87:2385–97.
28. Andreasen M, Hablitz JJ. Paired-pulse facilitation in the dentate gyrus: a patch-clamp study in rat hippocampus in vitro. J Neurophysiol. 1994;72:326–36.
29. Haorah J, Knipe B, Gorantla S, Zheng J, Persidsky Y. Alcohol-induced blood-brain barrier dysfunction is mediated via inositol 1,4,5-triphosphate receptor (IP3R)-gated intracellular calcium release. J Neurochem. 2007;100:324–36.
30. Medina KL, McQueeny T, Nagel BJ, Hanson KL, Schweinsburg AD, Tapert SF. Prefrontal cortex volumes in adolescents with alcohol use disorders: unique gender effects. Alcohol Clin Exp Res. 2008;32:386–94.
31. Schweinsburg BC, Alhassoon OM, Taylor MJ, Gonzalez R, Videen JS, Brown GG, et al. Effects of alcoholism and gender on brain metabolism. Am J Psychiatry. 2003;160:1180–3.
32. Squeglia LM, Schweinsburg AD, Pulido C, Tapert SF. Adolescent binge drinking linked to abnormal spatial working memory brain activation: differential gender effects. Alcohol Clin Exp Res. 2011;35:1831–41.
33. Daneman R, Zhou L, Agalliu D, Cahoy JD, Kaushal A, Barres BA. The mouse blood-brain barrier transcriptome: a new resource for understanding the development and function of brain endothelial cells. PLoS One. 2010;5:e13741.
34. Matsumoto-Okazaki Y, Furuse M, Kajiya K. Claudin-5 haploinsufficiency exacerbates UVB-induced oedema formation by inducing lymphatic vessel leakage. Exp Dermatol. 2012;21:557–9.
35. Chiu PS, Lai SC. Matrix metalloproteinase-9 leads to claudin-5 degradation via the NF-κB pathway in BALB/c mice with eosinophilic meningoencephalitis caused by Angiostrongylus cantonensis. PLoS One. 2013;8:e53370.
36. Aslam M, Ahmad N, Srivastava R, Hemmer B. TNF-alpha induced NFκB signaling and p65 (RelA) overexpression repress Cldn5 promoter in mouse brain endothelial cells. Cytokine 2012;57:269–75.
37. Villa A, Gelosa P, Castiglioni L, Cimino M, Rizzi N, Pepe G, et al. Sex-specific features of microglia from adult mice. Cell Rep. 2018;23:3501–11.
38. Alfonso-Loeches S, Pascual M, Guerri C. Gender differences in alcohol-induced neurotoxicity and brain damage. Toxicology 2013;311:27–34.
39. Pantoni L, Garcia JH, Gutierrez JA. Cerebral white matter is highly vulnerable to ischemia. Stroke 1996;27:1641–6. discussion 47
40. Jiang L, Shen F, Degos V, Schonemann M, Pleasure SJ, Mellon SH, et al. Oligogenesis and oligodendrocyte progenitor maturation vary in different brain regions and partially correlate with local angiogenesis after ischemic stroke. Transl stroke Res. 2011;2:366–75.
41. Arai K, Lo EH. Experimental models for analysis of oligodendrocyte pathophysiology in stroke. Exp Transl stroke Med. 2009;1:6.
42. Alix JJ. Recent biochemical advances in white matter ischaemia. Eur Neurol. 2006;56:74–7.
43. Somkuwar SS, Villalpando EG, Quach LW, Head BP, McKenna BS, Scadeng M, et al. Abstinence from ethanol dependence produces concomitant cortical gray matter abnormalities, microstructural deficits and cognitive dysfunction. Eur Neuropsychopharmacol. 2021;42:22–34.
44. McCarthy GM, Farris SP, Blednov YA, Harris RA, Mayfield RD. Microglial-specific transcriptome changes following chronic alcohol consumption. Neuropharmacology 2018;128:416–24.
45. Warden AS, Wolfe SA, Khom S, Varodayan FP, Patel RR, Steinman MQ, et al. Microglia control escalation of drinking in alcohol-dependent mice: genomic and synaptic drivers. Biol Psychiatry. 2020;88:910–21.
46. Sanchez-Alavez M, Nguyen W, Mori S, Wills DN, Otero D, Ehlers CL, et al. Time course of microglia activation and brain and blood cytokine/chemokine levels following chronic ethanol exposure and protracted withdrawal in rats. Alcohol 2019;76:37–45.
47. He J, Crews FT. Increased MCP-1 and microglia in various regions of the human alcoholic brain. Exp Neurol. 2008;210:349–58.
48. Nixon K, Kim DH, Potts EN, He J, Crews FT. Distinct cell proliferation events during abstinence after alcohol dependence: microglia proliferation precedes neurogenesis. Neurobiol Dis. 2008;31:218–29.
49. Chen Z, Tzima E. PECAM-1 is necessary for flow-induced vascular remodeling. Arteriosclerosis, thrombosis, Vasc Biol. 2009;29:1067–73.
50. Chen J, Leskov IL, Yurdagul A Jr, Thiel B, Kevil CG, Stokes KY, et al. Recruitment of the adaptor protein Nck to PECAM-1 couples oxidative stress to canonical NF-kappaB signaling and inflammation. Sci Signal. 2015;8:ra20.
51. Privratsky JR, Tourdot BE, Newman DK, Newman PJ. The anti-inflammatory actions of platelet endothelial cell adhesion molecule-1 do not involve regulation of endothelial cell NF-kappa B. J Immunol. 2010;184:3157–63.
52. Almendro N, Bellon T, Rius C, Lastres P, Langa C, Corbi A, et al. Cloning of the human platelet endothelial cell adhesion molecule-1 promoter and its tissue-specific expression. Struct Funct Charact J Immunol. 1996;157:5411–21.
53. Botella LM, Puig-Kroger A, Almendro N, Sanchez-Elsner T, Munoz E, Corbi A, et al. Identification of a functional NF-kappa B site in the platelet endothelial cell adhesion molecule-1 promoter. J Immunol. 2000;164:1372–8.
54. Feaver RE, Gelfand BD, Blackman BR. Human haemodynamic frequency harmonics regulate the inflammatory phenotype of vascular endothelial cells. Nat Commun. 2013;4:1525.
55. Crews FT, Lawrimore CJ, Walter TJ, Coleman LG Jr. The role of neuroimmune signaling in alcoholism. Neuropharmacology 2017;122:56–73.
56. Crews FT, Sarkar DK, Qin L, Zou J, Boyadjieva N, Vetreno RP. Neuroimmune function and the consequences of alcohol exposure. Alcohol Res: Curr Rev. 2015;37:331–41. 44-51
57. Abdollahi A, Hahnfeldt P, Maercker C, Gröne HJ, Debus J, Ansorge W, et al. Endostatin's antiangiogenic signaling network. Mol Cell. 2004;13:649–63.
58. Erickson EK, Blednov YA, Harris RA, Mayfield RD. Glial gene networks associated with alcohol dependence. Sci Rep. 2019;9:10949.
59. Escartin C, Galea E, Lakatos A, O'Callaghan JP, Petzold GC, Serrano-Pozo A, et al. Reactive astrocyte nomenclature, definitions, and future directions. Nat Neurosci. 2021;24:312–25.
60. Pekny M, Pekna M, Messing A, Steinhäuser C, Lee JM, Parpura V, et al. Astrocytes: a central element in neurological diseases. Acta Neuropathol. 2016;131:323–45.
61. Rao PS, Bell RL, Engleman EA, Sari Y. Targeting glutamate uptake to treat alcohol use disorders. Front Neurosci. 2015;9:144.
62. Hwa L, Besheer J, Kash T. Glutamate plasticity woven through the progression to alcohol use disorder: a multi-circuit perspective. F1000Research. 2017;6:298.
63. Roberto M, Varodayan FP. Synaptic targets: chronic alcohol actions. Neuropharmacology 2017;122:85–99.
64. Cifani C, Koya E, Navarre BM, Calu DJ, Baumann MH, Marchant NJ, et al. Medial prefrontal cortex neuronal activation and synaptic alterations after stress-induced reinstatement of palatable food seeking: a study using c-fos-GFP transgenic female rats. J Neurosci. 2012;32:8480–90.
65. Carpenter-Hyland EP, Chandler LJ. Adaptive plasticity of NMDA receptors and dendritic spines: implications for enhanced vulnerability of the adolescent brain to alcohol addiction. Pharm Biochem Behav. 2007;86:200–8.
66. Ninan I, Arancio O. Presynaptic CaMKII is necessary for synaptic plasticity in cultured hippocampal neurons. Neuron 2004;42:129–41.
67. Wang T, Hauswirth AG, Tong A, Dickman DK, Davis GW. Endostatin is a trans-synaptic signal for homeostatic synaptic plasticity. Neuron 2014;83:616–29.
68. Pasek JG, Wang X, Colbran RJ. Differential CaMKII regulation by voltage-gated calcium channels in the striatum. Mol Cell Neurosci. 2015;68:234–43.
69. Zhang Y, Zhang J, Jiang D, Zhang D, Qian Z, Liu C, et al. Inhibition of T-type Ca^{2+} channels by endostatin attenuates human glioblastoma cell proliferation and migration. Br J Pharm. 2012;166:1247–60.
70. Huang YH, Schlüter OM, Dong Y. Cocaine-induced homeostatic regulation and dysregulation of nucleus accumbens neurons. Behav Brain Res. 2011;216:9–18.
71. Natividad LA, Steinman MQ, Laredo SA, Irimia C, Polis IY, Lintz R, et al. Phosphorylation of calcium/calmodulin-dependent protein kinase II in the rat dorsal medial prefrontal cortex is associated with alcohol-induced cognitive inflexibility. Addict Biol. 2018;23:1117–29.
72. Kroener S, Mulholland PJ, New NN, Gass JT, Becker HC, Chandler LJ. Chronic alcohol exposure alters behavioral and synaptic plasticity of the rodent prefrontal cortex. PLoS ONE. 2012;7:e37541.
73. Zorumski CF, Mennerick S, Izumi Y. Acute and chronic effects of ethanol on learning-related synaptic plasticity. Alcohol 2014;48:1–17.
74. White AM, Matthews DB, Best PJ. Ethanol, memory, and hippocampal function: a review of recent findings. Hippocampus 2000;10:88–93.
75. Holmes A, Fitzgerald PJ, MacPherson KP, DeBrouse L, Colacicco G, Flynn SM, et al. Chronic alcohol remodels prefrontal neurons and disrupts NMDAR-mediated fear extinction encoding. Nat Neurosci. 2012;15:1359–61.
76. Cannady R, Nguyen T, Padula AE, Rinker JA, Lopez MF, Becker HC, et al. Interaction of chronic intermittent ethanol and repeated stress on structural and functional plasticity in the mouse medial prefrontal cortex. Neuropharmacology 2021;182:108396.
77. Karpyak VM, Geske JR, Colby CL, Mrazek DA, Biernacka JM. Genetic variability in the NMDA-dependent AMPA trafficking cascade is associated with alcohol dependence. Addict Biol. 2012;17:798–806.
78. Besheer J, Faccidomo S, Grondin JJ, Hodge CW. Regulation of motivation to self-administer ethanol by mGluR5 in alcohol-preferring (P) rats. Alcohol Clin Exp Res. 2008;32:209–21.
79. Basuroy S, Leffler CW, Parfenova H. CORM-A1 prevents blood-brain barrier dysfunction caused by ionotropic glutamate receptor-mediated endothelial oxidative stress and apoptosis. Am J Physiol Cell Physiol. 2013;304:C1105–15.
80. Betzen C, White R, Zehendner CM, Pietrowski E, Bender B, Luhmann HJ, et al. Oxidative stress upregulates the NMDA receptor on cerebrovascular endothelium. Free Radic Biol Med. 2009;47:1212–20.
81. Zhu HJ, Liu GQ. Glutamate up-regulates P-glycoprotein expression in rat brain microvessel endothelial cells by an NMDA receptor-mediated mechanism. Life Sci. 2004;75:1313–22.

82. Kim A, Zamora-Martinez ER, Edwards S, Mandyam CD. Structural reorganization of pyramidal neurons in the medial prefrontal cortex of alcohol dependent rats is associated with altered glial plasticity. Brain Struct Funct. 2015;220:1705–20.
83. Lee JH, Isayeva T, Larson MR, Sawant A, Cha HR, Chanda D, et al. Endostatin: a novel inhibitor of androgen receptor function in prostate cancer. Proc Natl Acad Sci USA. 2015;112:1392–7.
84. Walia A, Yang JF, Huang YH, Rosenblatt MI, Chang JH, Azar DT. Endostatin's emerging roles in angiogenesis, lymphangiogenesis, disease, and clinical applications. Biochim Biophys Acta. 2015;1850:2422–38.

ACKNOWLEDGEMENTS

The authors thank McKenzie Fannon, Nicole Phan, Kristen Peralta, Leon Quach, Joyee Tseng, Dr. Yoshio Takashima and Shaimaa Hassan for assistance with animal behavior and tissue processing. The authors thank Dr. John J. Woodward, MUSC, for helpful discussions on the electrophysiology data and analysis. Parts of this work was submitted in part as Master's Thesis by NX, AAS and TB to the Division of Biological Sciences, University of California, San Diego.

AUTHOR CONTRIBUTIONS

WT is deceased. Experimental design: YA, JCP, CDM; data collection- YA, ADK, NX, AAS, TB, JRW, BS, SSS, WT, SO; data analyses- YA, ADK, NX, AAS, TB, SO; writing, review & editing- YA, NX, AAS, TB, JCP, MR, CDM.

FUNDING

Funds from the National Institute on Alcoholism and Alcohol Abuse, National Institute on Drug Abuse (AA06420 to MR; AA020098 and DA034140 to CDM), and Department of Veterans Affairs (BX003304 to CDM) supported the study.

COMPETING INTERESTS

The authors declare no conflict of interest. The funders had no role in the design of the study; in the collection, analyses, or interpretation of data; in the writing of the manuscript, and in the decision to publish the results.

ADDITIONAL INFORMATION

Supplementary information The online version contains supplementary material available at https://doi.org/10.1038/s41386-021-01075-6.

Correspondence and requests for materials should be addressed to C.D.M.

Reprints and permission information is available at http://www.nature.com/reprints

Publisher's note Springer Nature remains neutral with regard to jurisdictional claims in published maps and institutional affiliations.